coatings

MDPI

Article

Optimization of LPCVD Deposition Conditions of Silicon-Rich Silicon Nitride to Obtain Suitable Optical Properties for Photoluminescent Coating

Francisco Uribe González [1,*], Karim Monfil Leyva [1,*], Mario Moreno Moreno [2], Alfredo Morales Sánchez [2], Ana L. Muñoz Zurita [3], José A. Luna López [1], Jesús Carrillo López [1], José A. D. Hernández de la Luz [1] and Alma S. L. Salazar Valdez [1]

[1] Researching Center on Semiconductor Devices, Meritorious University Autonomous of Puebla, Av. San Claudio s/n, Col. San Manuel, Puebla C.P. 72570, Mexico; jose.luna@correo.buap.mx (J.A.L.L.); jesus.carrillolopez@viep.com.mx (J.C.L.); jose.hernandez@correo.buap.mx (J.A.D.H.d.l.L.); alma.salazarva@alumno.buap.mx (A.S.L.S.V.)
[2] National Institute of Astrophysics, Optics and Electronics, Luis Enrique Erro 1, Puebla C.P. 72840, Mexico; mmoreno@inaoep.mx (M.M.M.); alfredom@inaoep.mx (A.M.S.)
[3] Electronics Faculty, Meritorious University Autonomous of Puebla, Av. San Claudio s/n, Col. San Manuel, Puebla C.P. 72570, Mexico; analuz.munoz@correo.buap.mx
* Correspondence: cross.ride1234@gmail.com (F.U.G.); karim.monfil@correo.buap.mx (K.M.L.)

Abstract: Silicon nitride is a commonly used material for ceramic applications and in the fabrication processes of integrated circuits (ICs). It has also increased in interest from the scientific community for use as a functional coating due to its physical, mechanical, electrical, and optoelectronic properties. In particular, silicon-rich silicon nitride (SRSN) has been considered in the photovoltaic industry as a down-conversion film for solar cells. In this work, SRSN films have been obtained by the Low-Pressure Chemical Vapor Deposition (LPCVD) technique at low to moderate deposition temperatures with a variation in the precursor gas pressure ratio. The SRSN films showed a wide photoluminescence (PL) in the visible region (without a high-deposition temperature or annealing process) and suitable optical properties (refractive index and absorption in the UV) to be used as photoluminescent coating on silicon solar cells. The absence of high-deposition temperatures could preserve the original structure of silicon solar cells, once the SRSN layer was applied. In addition, control of the reactive gas pressure ratio and deposition temperature showed an influence on the refractive index, the surface roughness, and the PL emission.

Keywords: silicon nitride; silicon-rich silicon nitride; refractive index; photoluminescent coating; down-conversion effect; optical properties

Citation: Uribe González, F.; Monfil Leyva, K.; Moreno Moreno, M.; Morales Sánchez, A.; Muñoz Zurita, A.L.; Luna López, J.A.; Carrillo López, J.; Hernández de la Luz, J.A.D.; Salazar Valdez, A.S.L. Optimization of LPCVD Deposition Conditions of Silicon-Rich Silicon Nitride to Obtain Suitable Optical Properties for Photoluminescent Coating. *Coatings* **2024**, *14*, 1383. https://doi.org/10.3390/coatings14111383

Academic Editor: Gergana Alexieva

Received: 9 September 2024
Revised: 19 October 2024
Accepted: 24 October 2024
Published: 31 October 2024

1. Introduction

Solar cells have become more prominent in the semiconductor market during the last decade; they have been continuously increasing in their relevance and impact on materials engineering and technology development. In the same way, the initial silicon solar cells with functional coatings have been investigated to improve efficiency and to reach higher competitive levels. In particular, the coatings used to create red-shift effects, which have shown important results, are among the recurrent add-ons [1,2]. Even different materials have been recently investigated to overcome optical loss by using them as antireflective coatings (ARCs), like silicon dioxide sol compositions, nanostructured TiO_2 or SiO_2/ITO, and ITO/TNO combinations [3–6]. However, silicon nitride (Si_3N_4) is a well-known material which has increased in interest from the industrial sector and the scientific community to be used as a functional coating due to its physical, mechanical, electrical, and optoelectronic properties [7–10]. Si_3N_4 was originally developed as a high-strength and high-toughness material, but recent reports have demonstrated that Si_3N_4

thin films are efficient and low-cost options to be used as an ARC [11–13]. Antireflective coatings should produce diffuse reflection and total internal reflection, but they should also preserve the properties of the materials on which they are deposited [14,15]. Si_3N_4 can be deposited using different techniques, such as Sputtering, Plasma-Enhanced Chemical Vapor Deposition (PECVD), Catalytic Chemical Vapor Deposition (Cat-CVD), Hot-Wire Chemical Vapor Deposition (HWCVD), etc. [16–19]. In particular, the physical properties of Si_3N_4 films can be varied by deposition temperature, growth time, and the ratio of the precursor gasses. When these Si_3N_4 films have been deposited at temperatures above 950 °C, they have shown interesting optical properties, but they have also faced some challenges when they are deposited on PN junctions. The deposition temperature of Si_3N_4 films is a very important parameter influencing their morphological, structural, and optical properties but the high-temperature deposition of these coatings on PN junctions can produce changes in the junction depth and consequently in the performance of solar cells [20–24]. On the other hand, these films have been deposited at unusually low temperatures, and their morphological, optical, and chemical characteristics have been clearly compromised [25,26]. In this way, the refractive index, root mean square roughness, and silicon excess of Si_3N_4 have shown an important dependence on deposition temperature, growth time, and the precursor gas ratio [10,16,27]. One possible alternative to preserve ARC characteristics in silicon nitride material and improve them with an effect of absorption on the UV range and emission in the visible region (down conversion) could be obtained with silicon-rich silicon nitride (SRSN or SiN_x) [28–30]. SRSN films can be obtained by LPCVD using a combination of NH_3 and SiH_4 as precursor gasses at temperatures usually above 725 °C. As-deposited SRSN films obtained by LPCVD have shown UV absorption and a wide photoluminescence (PL) spectrum in the visible range, where the maximum peak shifted from ∼490 to ∼590 nm as the silicon excess increased [31,32]. However, the behavior of these SRSN films not only depends on stoichiometry, but on all deposition conditions and thickness [21,33,34]. Information and interesting results of the SRSN films obtained by the PECVD technique have been reported by different authors [21,35,36], but SRSN films with interesting optical properties also can be obtained by a cheaper technique like LPCVD. In this way, an optimization on the deposition conditions of SRSN films obtained by LPCVD is required to obtain a suitable refractive index, roughness on the surface, and strong photoluminescence (PL) in the visible region even when SRSN films are deposited at moderate temperature ranges.

In this work, we provide a full description of the optimization of the deposition conditions like the deposition temperature and pressure gas ratio to obtain thin SRSN films by the LPCVD technique at temperatures $\leq$ 720 °C. No post-deposition thermal annealing was applied to the SRSN films. We provide an analysis of the optical, structural, and morphological characteristics from these SRSN films in order to control the thickness, refractive index, surface morphology, and PL emission. The optimization of the deposition conditions of the SRSN films allowed us to obtain suitable optical properties in this material to be applied as a photoluminescent coating.

2. Materials and Methods

SRSN films were deposited on p-type (100-oriented) silicon substrates with resistivity of 2–5 Ω cm by LPCVD. Before deposition, silicon wafers were cleaned using acetone, ethanol, and deionized water for 10 min followed by ultrasonic baths each, they were then cleaned with HF 10% (hydrofluoric acid) to remove native oxides, and finally, we used standard RCA solutions. The pressure ratio (Ro_N) of the reactive gasses (NH_3, SiH_4) was changed to increase the amount of silicon excess in the SRSN films in order to obtain optical characteristics like ARCs [12–15]. Ro_N is defined by Equation (1):

$$Ro_N = \frac{P(NH_3)}{P(SiH_4)} \quad (1)$$

Two sets of samples were obtained: The first set was obtained by fixing the deposition temperature at 720 °C, and Ro_N was changed in the range of 4 to 80. In the second set, we used a fixed Ro_N = 4, and different deposition temperatures were used in the range of 600 to 720 °C.

The thickness and refractive index of the SRSN films were calculated from measurements with a Gaertner L117 null ellipsometer (632.8 nm). Surface morphology was studied by atomic force microscopy measurements (AFM) using a Nanosurf EasyScan AFM system Version 2.3, operated in contact mode. A 450 µm long single-crystal Si cantilever operated at 12 kHz was used. AFM images were analyzed using the Scanning Probe Image Processor (SPIP) software 6.7.9. The SRSN vibrational modes were examined by Fourier Transform Infrared spectroscopy (FTIR) using a Bruker model Vector 22 (Coventry, UK) in the range of 400–4000 cm^{-1} and a 1 cm^{-1}/s resolution speed. Measurements of the chemical composition were obtained using Hitachi SU3500 SEM equipment (Tokyo, Japan) with an Electron Diffraction Spectroscopy (EDS) Bruker system operated at high vacuum. PL emission spectra were obtained with a Spectrofluorometer Fluoromax 3 Jobin Yvon (Horiba, NJ, USA) controlled with a computer. A set of filters were used to obtain only the UV excitation and visible emission. All SRSN films were excited using 270 nm radiation, and the PL emission signal was collected from 380 to 900 nm with a 1 nm/s resolution speed.

3. Results and Discussion

3.1. First Experiment

3.1.1. Refractive Index, Deposition Rate, and Pressure Ratio

In this section, we describe the obtained results of the SRSN films in order to control refractive index using a stable deposition ratio. The ratio of precursor gasses (Ro_N) was changed in the range of 4 to 80 to obtain SRSN films with a different refractive index. Figure 1a shows the relationship between the refractive index and the Ro_N at 720 °C. According to the refractive index value behavior, there is a limit on the atomic percentage of silicon excess introduced in SRSN films. In general, the thickness of the as-deposited SRSN films was calculated from ellipsometry measurements, and they showed a mean thickness of about 160 nm. The highest and lowest refractive indices were 2.21 and 1.98 when R_{ON} was 20 and 80, respectively.

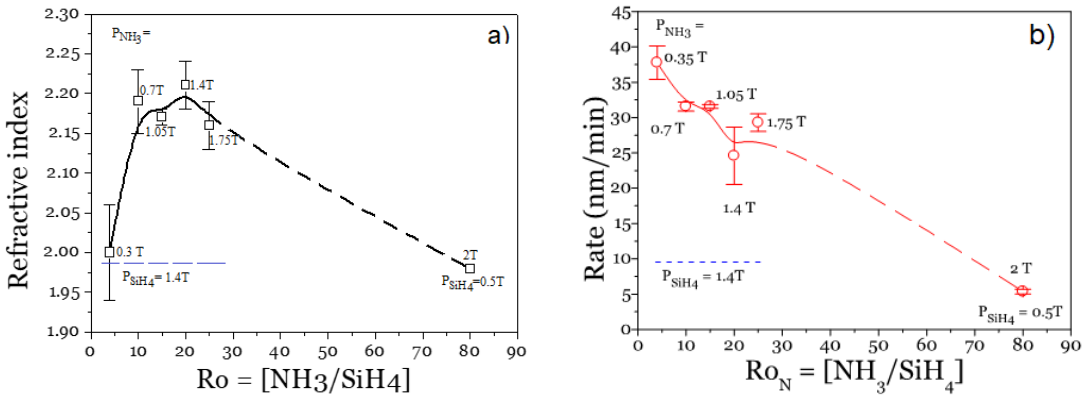

Figure 1. (**a**) Refractive index and (**b**) growth rate vs. pressure ratio R_{oN} of SRSN LPCVD at 720 °C.

In Figure 1b, we can observe the deposition ratio vs. the pressure ratio of the SRSN films. The pressure ratio was changed by adjusting the precursor gas ratio as indicated. The refractive index showed an increase from 2.01 to 2.20 in the range of Ro_N between 4 and 20 and a lineal decrease from 2.20 to 1.98 in the range of Ro_N from 20 to 80. According to Cheng et al. [37] and our results in Figure 1a, there is a clear tendency for the refractive index to decrease as the pressure ratio is increased. The deposition ratio showed an almost lineal decay from 37.5 to 5 nm/min in the range of $4 \leq Ro_N \leq 80$. Table 1 shows the main deposition characteristics of each SRSN film and its corresponding refractive index.

Table 1. Main deposition characteristics and refractive index for the first experiment.

Sample	NH_3 (Torr)	SIH_4 (Torr)	Ro_N	RATE (nm/min)	REFRACTIVE INDEX
LPC01	0.35	1.40	4	37.5	2.00
LPC02	0.70	1.40	10	32.5	2.19
LPC03	1.05	1.40	15	31.9	2.16
LPC04	1.40	1.40	20	24	2.21
LPC05	1.75	1.40	25	30	2.15
LPC06	2.00	0.50	80	5	1.98

According to these parameters, we obtained the lowest refractive index ($\leq$2.0) when the minimum and maxima Ro_N were used during deposition; a very similar growth rate was reached at both limits, around 5 nm/min. The refractive index was changed in all the ranges of $4 < Ro_N < 80$, because the change in silane pressure produced a change in composition and film stoichiometry. This will be discussed in EDS Results and Analysis of Vibrational Modes sections.

3.1.2. Refractive Index Selection

In order to select the optimal refractive index of the SRSN films to work as an antireflective coating, we performed some calculations, considering the blue- to red-shift effect. By considering the lowest refraction to use these films as ARCs, the refractive index can be calculated as follows [33]:

$$n_{arc} = \sqrt{n_0 n_s} = \sqrt{1.0002926 \cdot 4.01} = 2.002791 \quad (2)$$

where n_0 is the silicon reflective index and n_s is the antireflective coating reflective index. According to this calculation, we obtained only a refractive index (n_{SRSN}) of about 2.0 when $Ro_N = 4$ but n_{SRSN} was lower than 2 when $Ro_N = 80$ was used for deposition. In this case, a value of $Ro_N = 4$ produced an SRSN film with a refractive index closest to the calculated optimal value. This would be in agreement with a characteristic value for the reported refractive index of 2.01–2.05 for silicon nitride films obtained by CVD techniques [35–37].

The comparison between the refractive index of the SRSN films reported in Table 1 with the optimal refractive index calculation allowed us to select $R_{oN} = 4$ for the second experiment. The second experiment was designedto obtain silicon-rich silicon nitride with a refractive index of 2 and down conversion effect (photoluminescence) at the lowest temperature as possible.

3.2. Second Experiment

3.2.1. Thickness and Refractive Index Dependence on Temperature

We fixed the NH_3 and SiH_4 pressure at 0.35 and 1.4 Torr, respectively, to fix the pressure ratio at $Ro_N = 4$ to reproduce the refractive index closest to the optimal n_{arc}, but we varied the deposition temperature from 600 to 720 °C to obtain another group of SRSN films with photoluminescence at the lowest deposition temperature as possible. Table 2 shows the main deposition characteristics of each SRSN film for the second experiment.

Table 2. Main deposition characteristics for the second experiment.

Sample	Substrate	Ro_N	Thickness (nm)	Deposition Temperature (°C)	Growth Time (min)
LP21	2″ N + (2.0 Ω·cm)	4.00	75	600	5
LP22	2″ N + (2.0 Ω·cm)	4.00	95	650	5
LP23	2″ N + (2.0 Ω·cm)	4.00	112	700	5
LP24	2″ N + (2.0 Ω·cm)	4.00	250	720	5

We studied the temperature influence on thickness and refractive index by fixing the deposition time at 5 min. In Figure 2, we observed a clear dependence of thickness in temperature, where thickness was increased from 75 up to 250 nm according to the increase in deposition temperature from 600 up to 720 °C. According to Liu et al. [38], the growth rate of silicon nitride films obtained by LPCVD shows an Arrhenius behavior between 730 and 830 °C. In this case, the thickness of the silicon nitride samples should be clearly increased as the deposition temperature reaches 730 °C as with our SRSN sample obtained at 720 °C. We used the mean thickness values and the minimal squares theory in OriginPro 8.0 software to obtain a fitted curve that is directly proportional to the following equation:

$$\mathrm{Th(K)} = \mathrm{K}^3 - 0.91\mathrm{K}^2 + 587.71\mathrm{K} - 125955 \quad (3)$$

where Th = thickness and K = temperature.

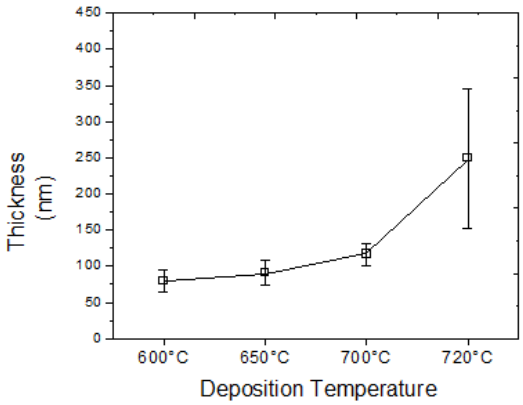

Figure 2. SRSN films thickness (nm) vs. deposition temperature (°C).

In the same way, we can observe in Figure 3 an inversely proportional dependence of the refractive index on deposition temperature, where the highest refractive index of 2.4 was obtained at a deposition temperature of 600 °C and decreased as temperature was increased. This would suggest that low-deposition temperature promotes non-stoichiometric silicon nitride content and high-deposition temperature enables an ordering of crystalline structure according to stoichiometric silicon nitride. Even when the same LPCVD equipment has been used to deposit the two series of samples, it is common that some optical, physical, or electrical properties are not exactly reproduced. However, according to Figure 3, the refractive index shows a decrease as deposition temperature is increased; this behavior is also related to an increase in crystallinity as a result of deposition temperature increments. In general, refractive index values are in a similar to that of silicon-rich nitride films deposited by different techniques and different deposition temperatures [30]. If we assumed n = refractive index and K = temperature, we could use the minimal squares approximation in the Origin Software again, and the obtained relationship is as follows:

$$n(K) = K^3 + 0.01K^2 - 3.72K + 805.15 \quad (4)$$

3.2.2. Refractive Index and Deposition Rate Dependence on Deposition Temperature

Figure 4 shows the deposition rate and refractive index dependence on temperature. In this case, we can observe that the growth rate was lower when 600 to 700 °C deposition temperatures were used, and it only increased when 720 °C was applied during deposition. The main values for the refractive index and growth rate can be seen at the intersection of both graphs; according to this, the best option to achieve the maximum growth rate with the best refractive index n_{arc} would be using a deposition temperature of 703 °C.

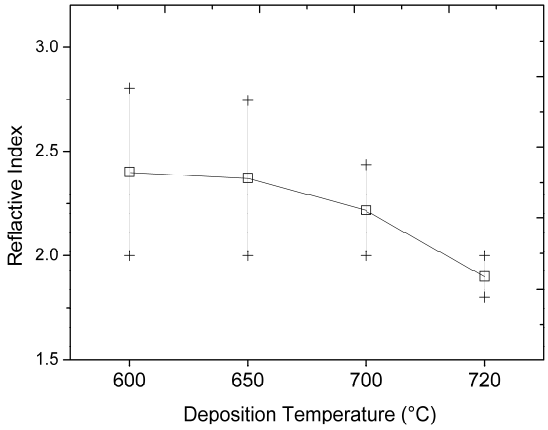

Figure 3. Refractive index vs. deposition temperature.

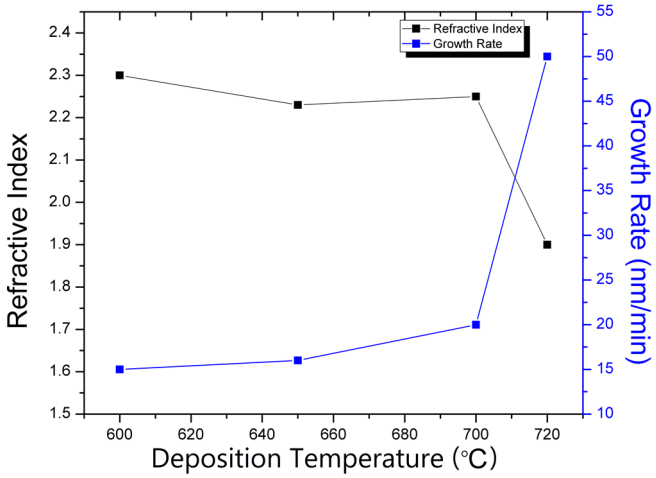

Figure 4. Relationship between refractive index and growth rate with deposition temperature.

3.3. EDS Results

We conducted a qualitative analysis of the elemental composition in our SRNS samples through EDS measurements from three different regions on the films' surfaces. An accelerating voltage of 0.5 kV was used to minimize damage to the SRSN films. Silicon, nitrogen, and oxygen elements in the SRSN films were confirmed from their characteristic X-ray peaks. The presence of a hydrogen peak in SRSN films cannot be determined because EDS can only provide information on the chemical composition for elements with atomic number (Z) > 3. A quantitative analysis could not be conducted for all SRSN films due to the thin thickness of the samples. The electrons from the primary beam of the Bruker system can penetrate 0.5 µm and interact with the atoms in SRSN films but also in silicon substrate. In this case, only EDS values for the SRNS film deposited at 720 °C (250 nm thickness) are shown in Table 3. The silicon value was around 60; meanwhile, nitrogen was approximately 25 at.%. The silicon composition value is close to stoichiometric silicon nitride (60.1 at.% for Si and 39.9 at.% for Ni), but the lowest value of nitride in the SRSN film would suggest a probable replacement by hydrogen atoms and would confirm the non-stoichiometric nature of this film. A previously reported analysis on the SRSN composition by means of XPS has also shown the presence of oxygen at the outmost part of the layer through the film depth, being present mainly at the film surface [21,35,36]. This behavior is similar in every SRSN film deposited at different deposition temperatures where a small value of oxygen was registered.

Table 3. EDS results from SRSN film with R_{oN} = 4 deposited at 720 °C.

Sample	Deposition Temperature (°C)	Silicon (At.%)	Nitrogen (At.%)	Oxygen (At.%)
LP24	720	60	25	2.56

3.4. Surface Morphology Dependence on Temperature

Surface morphology was studied through different roughness measurements obtained by AFM from each SRSN film. The root mean square (RMS) height (S_q) was calculated using SPIP software to analyze Tapping Mode AFM images [30,39]. Figure 5 shows S_q calculated results for the SRSN films deposited between 650 and 720 °C. The RMS values were around 2.5 and 6.8 nm on the SRSN films deposited in the range of 650 to 720 °C, respectively. A clear increase in RMS was observed as the deposition temperature was increased. In this case, an almost linear increasing dependance of S_q on the deposition temperature was obtained. The increase in the obtained RMS values could be related to the incorporation of nitrogen and hydrogen atomic content, as observed in the reported EDS values in Table 3. The replacement of silicon by nitrogen or hydrogen atoms produces different defects in the film, one of which is random roughness of the upper boundaries, with a consequent increase in RMS values. The standard deviation for SRSN films deposited at 650, 700, and 720 °C was less than 1 nm, as observed on the box plots, which indicates the homogeneity of our films deposited by LPCVD. According to the deposition parameters, the highest surface roughness and RMS height (S_q) were obtained when a high deposition temperature was used; this would have an influence (increase) on the reflectivity of the surface that could be achieved [39,40].

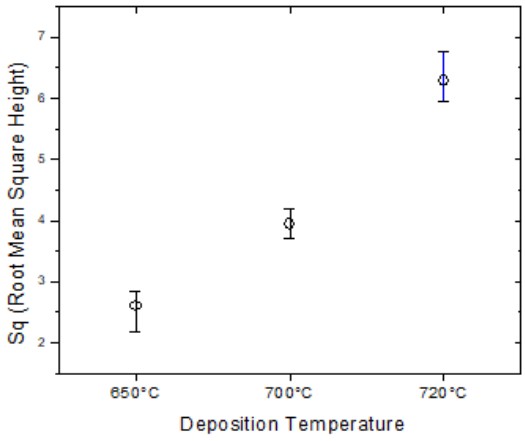

Figure 5. S_q (mean square height) and temperature dependence.

3.5. Photoluminescence

PL from the samples was measured to confirm and determine the peak of emission in the visible range. In Figure 6, we show a comparison of normalized PL from the SRSN film of R_{oN} = 80 deposited at 720 °C (SRSN80-720) with SRSN films of R_{oN} = 4 deposited at 700 (SRSN4-700) and 720 °C (SRSN4-720); all samples showed a clear PL with a main emission band centered around the green region. These samples were compared due to the similar refractive index observed in Table 1. The main difference between the PL spectra of SRSN80-720 in the first experiment and SRSN4 films for the second, was the beginning of the PL emission band, where the PL of the SRSN80-720 started at the visible region but emission from SRSN4 films begins at the UV region. Moreover, the SRSN4-700 and SRSN4-720 films showed the same emission peaks (identified in Figure 7), and some shifts from the usual pattern of silicon nitride films were identified. The main difference in PL between these films was the PL intensity on the emission centered around 478.1 nm (2.59 eV). Previous works have reported that oxygen in SRSN films (like SRSN4-700 and SRSN4-720) will create a gap state of Si–O above the VBM, which will produce an

electronic transition from the K^0 centers to ≡Si–O–Si, giving rise to the 478.1 nm (∼2.59 eV) emission [27,32].

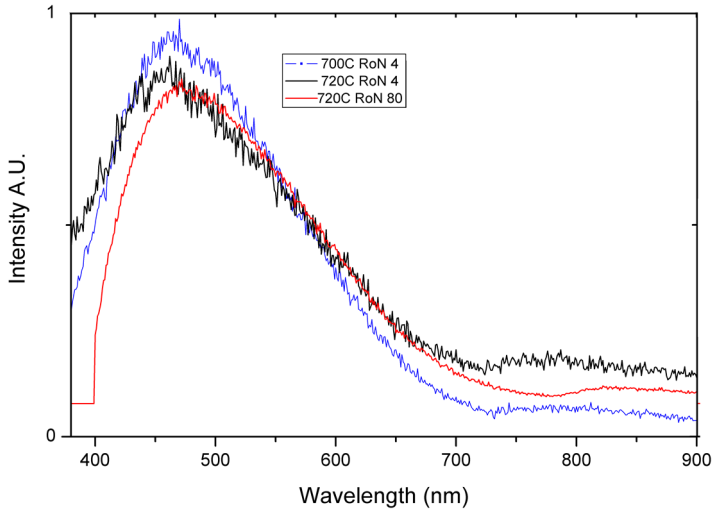

Figure 6. Photoluminescence spectra of SRSN films deposited at 700 and 720 °C.

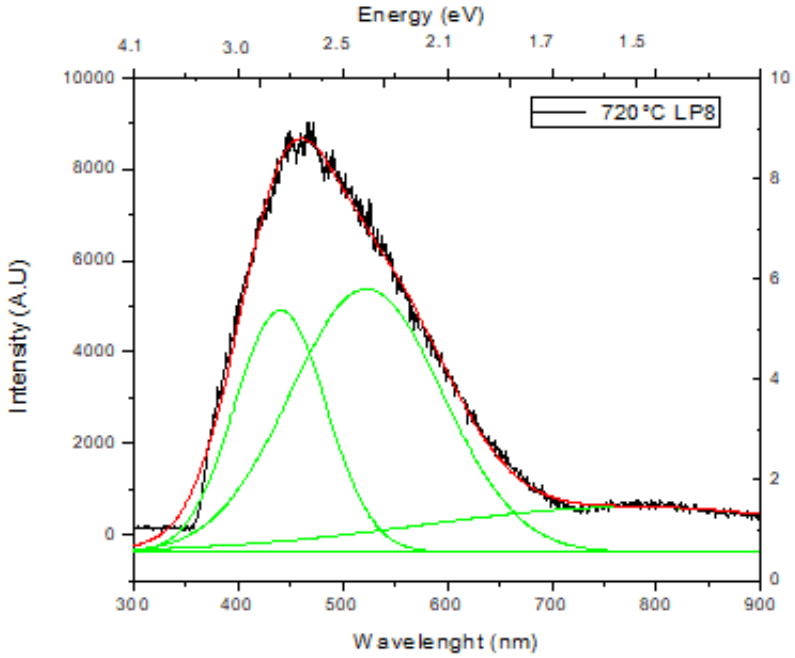

Figure 7. Deconvolution of photoluminescence of 720 °C sample.

According to the similar PL behavior for the SRSN4-700 and SRSN4-720 films, a detailed analysis was obtained only through the deconvolution of the PL from the SRSN film deposited at 720 °C, as shown in Figure 7. Three emission bands were identified, the first one in the near-infrared region (NIR), the second in the green region, and the last one in the blue region. In the first band, we obtained a low but non-negligible emission centered at 773.3 nm (1.6 eV); this could be considered in the range of reported photoluminescence of SiN_x films. There are many radiative defects that could be responsible for the emission in this region, even though this peak in strong emission has been attributed to the effect of luminescence from Si nanocrystals (nCs) embedded in this kind of matrix by other authors [41,42].

The emission in the NIR also has been attributed to the presence of Silicon Quantum Dots (Si-QDs) that can promote the *QCE* effect (quantum confinement effect). A low excess

of silicon in this sample (near or below stoichiometric silicon nitride), as shown in the EDS results, could be related to the main average size of the Si-QDs and, consequently, will be related to the observed PL emission [43–45]. However, further studies based on Transmittance Electron Microscopy will be required to confirm the presence of Si-nCs or Si-QDs.

The highest intensity of photoluminescence was found at 478.1 nm (2.59 eV) without symmetry in the emission band, which may be due to the size distribution of Si bonds and different species. This peak would be strongly influenced by the contribution of a radiative Si dangling bond K^0 center around 520 nm (2.39 eV) [46]. Finally, a strong emission peak is located in the blue region around 420 nm (2.81 eV), which may be due to a higher density of Si species than Si-N or an effect of surface passivation decreasing dangling bonds and increasing radiative recombination centers [46–49]. A correlation between the PL peak energy with the optical bandgap indicates that the luminescence is related to the band tail carrier recombination in the SRSN films.

Optimal Thickness Calculation

The optical thickness to produce down conversion using SRSN films needs to be calculated. The optimum optical thickness must be chosen like an antireflective coating (ARC) for an optimal energy conversion, so the optimum optical thickness was calculated based on the Fresnel equation for reflection theory [50] as follows:

$$R = |1 - T| = \frac{a_1 cos^2\delta_1 + a_2 sen^2\delta_1}{a_3 cos^2\delta_1 + a_4 sen^2\delta_1} \quad (5)$$

The following equation was obtained:

$$\frac{\delta_1 \lambda}{2\pi} = n_{arc} t_{arc} \quad (6)$$

$$\delta_1 = \frac{2\pi}{\lambda} n_{arc} t_{arc} \quad (7)$$

where δ_1 is the phase difference introduced by the antireflective layer, λ is the incident wavelength, n_{arc} is the refractive index of the layer, and t_{arc} is its thickness. According to antireflection coating theory and using δ_1 = 0.5 π, in most cases of interest, R vanishes when

$$t_{arc} = \frac{\lambda}{4n_{arc}}; \frac{3\lambda}{4n_{arc}}; \frac{5\lambda}{4n_{arc}} \ldots \quad (8)$$

Then, we used the calculated optimal refractive index (n_{arc}) and the Fresnel equation to obtain a suitable thickness with a red-shift effect (down conversion) [3,4,12,15,27,33] in the visible spectrum. In this way, looking for the film to absorb or transmit radiative energy with the expected down-conversion effect, we used the obtained wavelength of the highest PL peak from our SRSN films at λ = 478.1 nm, and then, 478.1 nm/(4 × 2.002) = t_{arc}. The optimal thickness of the film for emission around 478.1 nm should be $\boldsymbol{t_{arc}} \approx$ 60 nm.

3.6. Analysis of Vibrational Modes

Vibrational modes were identified by means of the obtained FTIR absorbance spectra of our SRSN films. Figure 8 shows a comparison of absorbance spectra of the SRSN films deposited at 700 °C and 720 °C; a deconvolution was carried out to locate the main peaks related to vibrational modes. In both samples, we could observe the conventional vibrations of silicon nitride corresponding to 960 and 1300 cm^{-1} [51,52].

For the SRSN film deposited at 720 °C, we can observe a strong peak for the Si-H "Wagging" mode at 625 cm^{-1} in (label A). In the same way, we can observe a clear and characteristic peak of the Si_3N_4 to Si-N_3-H "Asymmetric Stretching" mode at 960 cm^{-1} peak (label C) for both samples, which has been related to Si_xN_y species; then, a non-stoichiometric behavior could be confirmed according to the PL emission peaks, atomic

content in Table 3, and previous reported films obtained at similar conditions but different deposition temperatures [52–55]. The presence of different Si_xN_y species confirms the relationship with the observed PL around 2.77 eV.

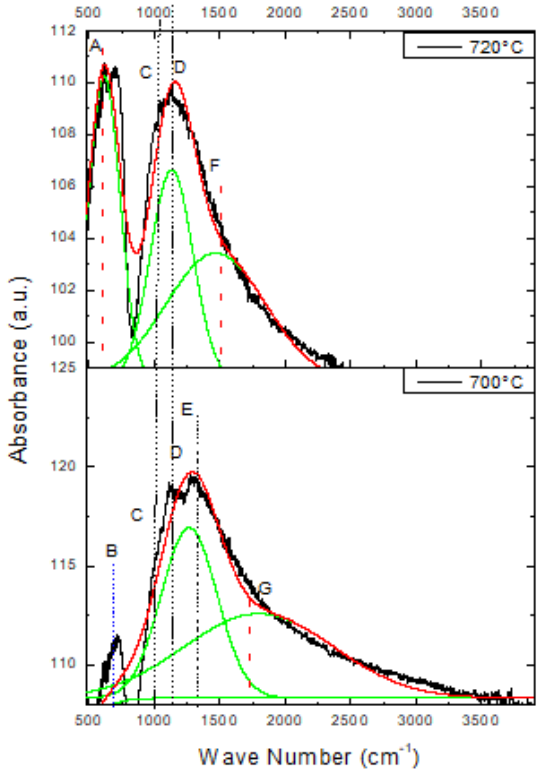

Figure 8. FTIR absorbance spectra of SRSN films deposited at 700 °C and 720 °C.

For the SRSN film obtained at 700 °C, we can observe a vibrational mode from 650 to 790 cm^{-1} with a centered peak around 690 cm^{-1} corresponding to Si-H and Si-N-H (label B) [52]. These species can be related to the deposition process without thermal annealing (as-deposited) and the off-stoichiometry nature in SRSN films with hydrogen enrichment [26,32,47] regarding the PL and EDS results. In the same way, there is a peak centered around 1010 cm^{-1} (label C), where we observe a lower intensity peak in this film than that obtained from the 720 °C sample. This peak represents the Si-N "Asymmetric Stretching" mode but has also been related to H-Si-N_3 species [52,56]. The observed peak in both SRSN films around 1260 cm^{-1} (label D-E) can be related to the H-N_3 and N-H Wagging mode. [48,49]. Also, 1550 cm^{-1} (label F) can be related to the Wagging N-H vibration mode [55]. The Si-H Wagging mode [52,56], which has been related to the band centered at 1850 cm^{-1} (label G) [57], could be due to the great abundance of hydrogen in our films produced by the silane precursor during the deposition process, as suggested by the EDS results.

Regarding the small difference in the intensity between the A and B labels, which correspond to Si-H, we can relate this variation to the small increase in deposition temperature from 700 to 720 °C. The hydrogen species predominating in the 720 °C sample can usually be removed by thermal treatments; however, our SRSN films did not have any annealing treatment to avoid N-H or Si-H species [51,52,57]. The absence of high-deposition temperatures or annealing treatments could preserve the original structure of silicon solar cells where the SRSN layer would be applied on top.

4. Conclusions

Silicon-rich silicon nitride films can be obtained by the LPCVD technique at temperatures under 720 °C in order to avoid physical changes in semiconductor junctions

when they are applied as an antireflective coating on devices. SRSN films deposited at temperatures below 720 °C showed a refractive index in the range of 2.0 to 2.2 to be used as an antireflective coating. A mean square roughness from 2.5 to 6.5 nm with an almost linear increasing dependance of S_q on deposition temperature was obtained due to an increase in nitrogen and hydrogen content. The SRSN films showed a strong PL in the blue to red region without any kind of post-deposition annealing. The vibrational modes related to Si_3N_4, Si-N_3-H, and Si-N-H corroborate the off-stoichiometry nature and nitrogen enrichment in our SRSN films. The radiative defects produced by Si_xN_y species and QCE were related to the observed PL bands. According to the relationship of the growth rate and refractive index on the temperature and precursor gas ratio, the thickness and optical characteristics of the SRSN films can be controlled for application as a photoluminescent coating.

Author Contributions: Conceptualization, F.U.G., K.M.L. and A.L.M.Z.; methodology, F.U.G., K.M.L., and A.L.M.Z.; software, F.U.G.; validation, F.U.G., K.M.L., M.M.M., and A.L.M.Z.; formal analysis, F.U.G., K.M.L., M.M.M., A.M.S., A.L.M.Z., and J.A.D.H.d.l.L.; investigation, J.A.L.L., J.C.L., J.A.D.H.d.l.L., and A.S.L.S.V.; resources, K.M.L., M.M.M., A.M.S., J.A.L.L., J.C.L., and J.A.D.H.d.l.L.; writing—original draft preparation, F.U.G., K.M.L., M.M.M., and A.L.M.Z.; writing—review and editing, F.U.G., K.M.L., M.M.M., A.M.S., A.L.M.Z., J.A.L.L., J.C.L., J.A.D.H.d.l.L., and A.S.L.S.V.; supervision K.M.L., M.M.M., and A.L.M.Z. All authors have read and agreed to the published version of the manuscript.

Funding: This work has been partially supported by CONAHCyT [grant number: 217570727] and 100520056-VIEP2024 project.

Institutional Review Board Statement: Not applicable.

Informed Consent Statement: Not applicable.

Data Availability Statement: Data are contained within the article.

Acknowledgments: The authors acknowledge CIDS, INAOE, and IER laboratories for their help in the samples' obtention and characterization.

Conflicts of Interest: The authors declare no conflicts of interest.

References

1. Luft, W. Effects of electron irradiation on N on P silicon solar cells. *Adv. Energy Convers.* **1965**, *5*, 21–41. [CrossRef]
2. Shah, A. Thin-Film Silicon Solar Cells. In *Practical Handbook of Photovoltaics*; Elsevier: Amsterdam, The Netherlands, 2012; pp. 209–281. [CrossRef]
3. Lokteva, A.A.; Kotelnikova, A.A.; Kovylin, R.S.; Konev, A.N.; Piskunov, A.V. Novel Antireflection Coatings Obtained by Low-Temperature Annealing in the Presence of Tetrabutylammonium Bromide and Gold Nanoparticles. *Materials* **2022**, *15*, 7658. [CrossRef] [PubMed]
4. Abu-Shamleh, A.; Alzubi, H.; Alajlouni, A. Optimization of antireflective coatings with nanostructured TiO_2 for GaAs solar cells. *Photonics Nanostruct. Fundam. Appl.* **2021**, *43*, 100862. [CrossRef]
5. Ho, W.-J.; Lin, J.-C.; Liu, J.-J.; Bai, W.-B.; Shiao, H.-P. Electrical and Optical Characterization of Sputtered Silicon Dioxide, Indium Tin Oxide, and Silicon Dioxide/Indium Tin Oxide Antireflection Coating on Single-Junction GaAs Solar Cells. *Materials* **2017**, *10*, 700. [CrossRef]
6. Lee, Y.S.; Chuang, L.Y.; Tang, C.J.; Yan, Z.Z.; Le, B.S.; Jaing, C.C. Investigation into the Characteristics of Double-Layer Transparent Conductive Oxide ITO/TNO Anti-Reflection Coating for Silicon Solar Cells. *Crystals* **2023**, *13*, 80. [CrossRef]
7. Bocanegra-Bernal, M.H.; Matovic, B. Mechanical properties of silicon nitride-based ceramics and its use in structural applications at high temperatures. *Mater. Sci. Eng. A* **2010**, 1314–1338. [CrossRef]
8. Nguyen, V.S.; Burton, S.; Pan, P. The Variation of Physical Properties of Plasma-Deposited Silicon Nitride and Oxynitride with Their Compositions. *J. Electrochem. Soc.* **1984**, *131*, 2348. [CrossRef]
9. De Brito Mota, F.; Justo, J.F.; Fazzio, A. Structural and electronic properties of silicon nitride materials. *Int. J. Quant. Chem.* **1998**, *70*, 973–980. [CrossRef]
10. Beliaev, L.Y.; Shkondin, E.; Lavrinenko, A.V.; Takayama, O. Optical, structural and composition properties of silicon nitride films deposited by reactive radio-frequency sputtering, low pressure and plasma-enhanced chemical vapor deposition. *Thin Solid Films* **2022**, *763*, 139568. [CrossRef]

11. Tahir, S.; Saeed, R.; Ashfaq, A.; Ali, A.; Mehmood, K.; Almousa, N.; Shokralla, E.A.; Macadangdang, R.R., Jr.; Soeriyadi, A.H.; Bonilla, R.S. Optical modeling and characterization of bifacial SiNx/AlOx dielectric layers for surface passivation and antireflection in PERC. *Prog. Photovolt. Res. Appl.* **2024**, *32*, 63–72. [CrossRef]
12. Lelièvre, J.-F.; Kafle, B.; Saint-Cast, P.; Brunet, P.; Magnan, R.; Hernandez, E.; Pouliquen, S.; Massines, F. Efficient silicon nitride SiNx:H antireflective and passivation layers deposited by atmospheric pressure PECVD for silicon solar cells. *Progress. Photovolt.* **2019**, *27*, 1007–1019. [CrossRef]
13. Yu, J.; Daoming, Y.; Yingchun, C.; Wentao, G.; Manqing, T. High-performance SiO_2-SiN_X distributed Bragg reflectors fabricated by ion-assisted reactive magnetron sputtering. *Vacuum* **2024**, *220*, 112775. [CrossRef]
14. Lee, Y.; Gong, D.; Balaji, N.; Lee, Y.J.; Yi, J. Stability of SiN_X/SiN_X double stack antireflection coating for single crystalline silicon solar cells. *Nanoscale Res. Lett.* **2012**, *7*, 50. Available online: http://www.nanoscalereslett.com/content/7/1/50 (accessed on 2 September 2024). [CrossRef]
15. Sharma, R. Silicon nitride as antireflection coating to enhance the conversion efficiency of silicon solar cells. *Turk. J. Phys.* **2018**, *42*, 350–355. [CrossRef]
16. Guler, I. Optical and structural characterization of silicon nitride thin films deposited by PECVD. *Mater. Sci. Eng. B* **2019**, *246*, 21–26. [CrossRef]
17. TuHuynh, T.C.; Keisuke, O. Long-term stability of low-temperature deposited Cat-CVD SiNx thin film against damp-heat stress. *Jpn. J. Appl. Phys.* **2024**, *63*, 01SP25. [CrossRef]
18. Verlaan, V.; Van Der Werf, C.H.M.; Houweling, Z.S.; Romijn, I.G.; Weeber, A.W.; Dekkers, H.F.W.; Goldbach, H.D.; Schropp, R.E.I. Multi-crystalline Si solar cells with very fast deposited (180 nm/min) passivating hot-wire CVD silicon nitride as antireflection coating. *Prog. Photovolt. Res. Appl.* **2007**, *15*, 563–573. [CrossRef]
19. Alain, E.K.; Jové, F.A.; Goff, J.; Arkles, B. Silicon Nitride and Silicon Nitride-Rich Thin Film Technologies: Trends in Deposition Techniques and Related Applications. *ECS J. Solid State Sci. Technol.* **2017**, *6*, P691. [CrossRef]
20. Jones, S.W. Difussion in Silicon. 2008 IC Knowledge LLCC. Available online: https://api.semanticscholar.org/CorpusID:14437811 (accessed on 5 September 2024).
21. Braña, A.F.; Gupta, H.; Bommali, R.K.; Srivastava, P.; Ghosh, S.; Casero, R.P. Enhancing efficiency of c-Si solar cell by coating nano structured silicon rich silicon nitride films. *Thin Solid Films* **2018**, *662*, 21–26. [CrossRef]
22. Ali, R.M.; Zahran, M.B.; Youssif, A.M.; Eliwa, A. Characterization of Monocrystalline Silicon Solar Cells based on the Phosphorus Diffusion Temperature. *Int. J. Eng. Sci. Invent.* **2021**, *10*, 01–07. [CrossRef]
23. de la Mora, M.B.; Amelines-Sarria, O.; Monroy, B.M.; Hernández-Pérez, C.D.; Lugo, J.E. Materials for down conversion in solar cells: Perspectives and challenges. *Sol. Energy Mater. Sol. Cells* **2017**, *165*, 59–71. [CrossRef]
24. El amrani, A.; Menous, I.; Mahiou, L.; Tadjine, R.; Touati, A.; Lefgoum, A. Silicon nitride film for solar cells. *Renew. Energy* **2008**, *33*, 2289–2293. [CrossRef]
25. Jana, T.; Mukhopadhyay, S.; Ray, S. Low temperature silicon oxide and nitride for surface passivation of silicon solar cells. *Sol. Energy Mater. Sol. Cells* **2002**, *71*, 197–211. [CrossRef]
26. Hendawi, R.; Ciftja, A.; Stokkan, G.; Arnberg, L.; Di Sabatino, M. The effect of preliminary heat treatment on the durability of reaction bonded silicon nitride crucibles for solar cells applications. *J. Cryst. Growth* **2020**, *542*, 125670. [CrossRef]
27. Sahouane, N.; Zerga, A. Optimization of antireflection multilayer for industrial crystalline silicon solar cells. *Energy Procedia* **2014**, *44*, 118–125. [CrossRef]
28. Torchynska, T.V.; Espinola, J.L.C.; Khomenkova, L.; Hernandez, E.V.; Adame, J.A.A.; Slaoui, A. Structural and light emitting properties of silicon-rich silicon nitride films grown by plasma enhanced-chemical vapor deposition. *Mater. Sci. Semicond. Process.* **2015**, *37*, 46–50. [CrossRef]
29. Cabañas-Tay, S.A.; Palacios-Huerta, L.; Aceves-Mijares, M.; Coyopol, A.; Morales-Morales, F.; Pérez-García, S.A.; Licea-Jiménez, L.; Domínguez-Horna, C.; Monfil-Leyva, K.; Morales-Sánchez, A. Study of narrow and intense UV electroluminescence from ITO/SRO/Si-p and ITO/SRN/SRO/Si-p based lightemitting capacitors. *J. Lumin.* **2017**, *183*, 334–340. [CrossRef]
30. Yoshinaga, S.; Ishikawa, Y.; Kawamura, Y.; Nakai, Y.; Uraoka, Y. The optical properties of silicon-rich silicon nitride prepared by plasma-enhanced chemical vapor deposition. *Mater. Sci. Semicond. Process.* **2019**, *90*, 54–58. [CrossRef]
31. Kaloyeros, A.; Pan, Y.; Goff, J.; Arkles, B. Review—Silicon Nitride and Silicon Nitride-Rich Thin Film Technologies: State-of-the-Art Processing Technologies, Properties, and Applications. *ECS J. Solid State Sci. Technol.* **2020**, *9*, 063006. [CrossRef]
32. Bommali, R.; Preet, S.; Rai, S.; Mishra, P.; Sekhar, B.; Prakash, V.G.; Srivastava, P. Excitation dependent photoluminescence study of Si-rich a-SiNx:H thin films. *J. Appl. Phys.* **2012**, *112*, 123518. [CrossRef]
33. Mamgain, S. Structural and optical study of amorphous hydrogenated silicon nitride thin film as antireflection coating on solar cell. *Adv. Mater. Proc.* **2017**, *2*, 570–574. [CrossRef]
34. Rezgui, B.; Sibai, A.; Nychyporuk, T.; Lemiti, M.; Brémond, G. *Photoluminescence and Optical Absorption Properties of Silicon Quantum Dots Embedded in Si-Rich Silicon Nitride Matrices*; Elsevier: Amsterdam, The Netherlands, 2009. [CrossRef]
35. Liao, W.; Zeng, X.; Wen, X.; Zheng, W.; Yao, W. Synthesis and Optical Properties of Si-Rich Containing Silicon Quantum Dots. *J. Electron. Mater.* **2013**, *42*, 3445–3450. [CrossRef]
36. Takeoda, S.; Fujii, M.; Hayashi, S. Size-dependent photoluminescence from surface-oxidized Si nanocrystals in a weak confinement regime. *Phys. Rev. B* **2000**, *62*, 16820–16825. [CrossRef]

37. Cheng, Y.T.; Ho, J.J.; Lee, W.J.; Tsai, S.Y.; Lu, Y.A.; Liou, J.J.; Chang, S.H.; Wang, K.L. Investigation of Low-Cost Surface Processing Techniques for Large-Size Multicrystalline Silicon Solar Cells. *Int. J. Photoenergy* **2010**, 268035. [CrossRef]
38. Liu, X.J.; Zhang, J.J.; Sun, X.W.; Pan, Y.B.; Huang, L.P.; Jin, C.Y. Growth and properties of silicon nitride films prepared by low pressure chemical vapor deposition using trichlorosilane and ammonia. *Thin Solid Films* **2004**, *460*, 72–77. [CrossRef]
39. Komarov, F.F.; Parkhomenko, I.N.; Vlasukova, L.A.; Milchain, O.V.; Togambayeva, A.K.; Kovalchuck, N.S. Annealing Effects on Photoluminescence of SiNx films grown by PECVD. In Proceedings of the 10th International Conference: "Interaction of radiation with solids", Minsk, Belarus, 24–27 September 2013; pp. 238–241, ISBN 978-985-553-141-9.
40. Sharma, V.; Tracy, C.; Schroder, D.; Heresimenka, S.; Dauksher, W.; Bowden, S. Manipulation of K Center Charge Staates in silicon nitride films to achieve excellent Surface passivation for silicon solar cells. *Appl. Phys. Lett.* **2014**, *104*, 053503. [CrossRef]
41. Kilian, S.O.; Wiggers, H. Gas-Phase Synthesis of Silicon-Rich Silicon Nitride Nanoparticles for High Performance Lithium–Ion Batteries. *Part. Part. Syst. Charact.* **2021**, *38*, 2100007. [CrossRef]
42. Zhingunov, D.M.; Popov, A.A.; Chesnokov, Y.M.; Vasiliev, A.L.; Lebedev, A.M.; Subbotin, I.A.; Yakunin, S.N.; Shalygina, O.A.; Kamenskikh, I.A. Near-IR Emitting Si Nanocrystals Fabricated by thermal Annealing of SiNx/Si_3N_4 Multilayers. *App. Sci.* **2019**, *9*, 4725. [CrossRef]
43. Chen, X.; Yang, W.; Yang, P.; Yuan, J.; Zhao, F.; Hao, J.; Tang, Y. Size-controlled Si Quantum dots embedded in B-doped SiNx/Si_3N_4 superlatice for Si quantum dot solar cells. *J. Mater. Sci. Mater. Electron.* **2017**, *28*, 1322–1327. [CrossRef]
44. So, Y.-H.; Huang, S.; Conibeer, G.; Green, M.A. Formation and Photoluminiscence of Si nanocrystals in solid films. *Thin Solid Films* **2011**, *519*, 5408–5412. [CrossRef]
45. Linnros, J.; Lalic, N.; Galeckas, A.; Grivickas, V. Analysis of the stretched exponential photoluminescence decay from nanometer-sized silicon crystals in SiO2. *J. Appl. Phys.* **1999**, *86*, 6128–6134. [CrossRef]
46. Wang, M.; Li, D.; Yuan, Z.; Yang, D.; Que, D. Photoluminescence of Si-rich silicon nitride: Defect-related states and silicon nanoclusters. *Appl. Phys. Lett.* **2007**, *90*, 131903. [CrossRef]
47. Esposito, E.M.; Mercado, L.V.; Veneri, P.D.; Lancellotti, L.; Privato, C. *Annealing Effects on PECVD-Grown Si rich aSiNx Thin Films*; Elsevier: Amsterdam, The Netherlands, 2009. [CrossRef]
48. Deshpande, S.V. Optical properties of silicon nitride films deposited by hot filament chemical vapor deposition. *J. Appl. Phys.* **1995**, *77*, 6534–6541. [CrossRef]
49. Ko, C. Annealing effects on the photoluminescence of amorphous silicon-nitride films. *J. Korean Phys. Soc.* **2006**, *48*, 1277–1280.
50. Valiei, M.; Shaibani, P.M.; Abdizadeh, H.; Kolahdouz, M.; Soleimani, E.A.; Poursaf, J. Design and optimization of single, double and multilayer anti-reflection coatings on planar and textured surface of silicon solar cells. *Mater. Today Commun.* **2022**, *32*, 104144. [CrossRef]
51. Bugaev, K.O.; Zelenina, A.A.; Volodin, V.A. Vibrational Spectroscopy of Chemical Species in Silicon and Silicon-Rich Nitride Thin Films, Russian Academy of Sciences, Novosibirsk 63090, Russia. *Int. J. Spectrosc.* **2011**, *2012*, 2011. [CrossRef]
52. Scardera, G.; Puzzer, T.; Conibeer, G.; Green, M. Fourier transform infrared spectroscopy of annealed silicon-rich silicon nitride thin films. *J. Appl. Phys.* **2008**, *104*, 104310. [CrossRef]
53. Hoyos-García, J.E. Caracterización óptica y morfológica de partículas de silicio en una matriz SiNx obtenidas por PECVD, Instituto Politécnico Nacional. 2006. Available online: http://tesis.ipn.mx (accessed on 6 September 2024).
54. Nekrashevich, S.S.; Shaposhnikov, A.V.; Gritsenko, V.A. Study of the atomic and electronic structures of amorphous silicon nitride and defects in it, institute of semiconductor physics. *JETP Lett.* **2011**, *94*, 202–205. [CrossRef]
55. Torchynska, T.; Khomenkova, L.; Slaqui, A. Modification of light Emission in Si. Rich Silicon Nitride Films Versus Stoichiometry and Excitation light Energy. *J. Electron. Mater.* **2018**, *47*, 3927–3933. [CrossRef]
56. Xie, M.; Li, D.; Wang, F.; Yang, D. Luminescence Properties of Silicon-Rich Silicon Nitride Films and Light Emitting Devices. *ECS Trans.* **2011**, *35*, 3–19. [CrossRef]
57. Ahmed, N.; Singh, C.B.; Bhattacharya, S.; Dhara, S.; Bhargav, P.B. Raman and FTIR Studies on PECVD Grown Ammonia-Free Amorphous Silicon Nitride Thin Films for Solar Cell Applications. *Conf. Pap. Sci.* **2013**, *2013*, 837676. [CrossRef]